Available online at www.sciencedirect.com

ScienceDirect

Advances in Space Research 52 (2013) 2215–2225

ADVANCES IN SPACE RESEARCH (a COSPAR publication)

www.elsevier.com/locate/asr

Application of hybrid regularization method for tomographic reconstruction of midlatitude ionospheric electron density

Yibin Yao [a,b,*], Jun Tang [a], Jian Kong [a,c], Liang Zhang [a], Shun Zhang [a]

[a] School of Geodesy and Geomatics, Wuhan University, Wuhan 430079, China
[b] Key Laboratory of Geospace Environment and Geodesy, Ministry of Education, Wuhan University, Wuhan 430079, China
[c] School of Earth Science, Ohio State University, 1739 North High Street, Columbus, OH, USA

Received 18 June 2013; received in revised form 14 September 2013; accepted 24 September 2013
Available online 1 October 2013

Abstract

Reconstructing ionospheric electron density (IED) is an ill-posed inverse problem, with classical Tikhonov regularization tending to smooth IED structures. By contrast, total variation (TV) regularization effectively resists noise and preserves discontinuities of the IED. In this paper, we regularize the inverse problem by incorporating both Tikhonov and TV regularization. A specific formulation of the proposed method, called hybrid regularization, is introduced and investigated. The method is then tested using simulated data for the actual positions of the GPS satellites and ground receivers, and also applied to the analysis of real observation data under quiescent and disturbed ionospheric conditions. Experiments demonstrate the effectiveness, and illustrate the validity and reliability of the proposed method.

Keywords: Ionospheric tomography; Ill-posed inverse problem; Tikhonov regularization; Total variation regularization; Hybrid regularization

1. Introduction

The ionosphere is an important part of the geospace environment. Ionosphere monitoring technology is critical to the development of ionospheric theory and its applications.

Global Positioning System (GPS), a commonly used space geodetic techniques, is used to measure ionospheric delay and estimate electron density. Austen et al. (1986, 1988) first proposed the tentative idea of ionospheric imaging using computerized tomography (CT) and then employed computerized ionospheric tomography (CIT) technique to reconstruct ionospheric electron density (IED) profiles. Subsequently, various related experimental and theoretical studies have been conducted worldwide (Arikan et al., 2007; Hirooka et al., 2011; Hobiger et al., 2008; Ma and Maruyama, 2005; Mitchell and Spencer, 2003; Pryse et al., 1998; Raymund et al., 1990; Wen et al., 2007, 2008). Many researchers have proposed various CIT inversion algorithms which can be classified into iterative and non-iterative algorithms. The former includes the Algebraic Reconstruction Technique (ART), Multiplicative ART (MART), and Simultaneous Iteration Reconstruction Technique (SIRT). The latter includes the regularization method and the singular value decomposition (SVD) algorithm. However, during CIT, the inverse problem is ill-posed, and regularization functions are used to constrain the solution because of a lack of observation information and the presence of noise. Nygren(1997) used the regularization function combined variance information to reconstruct IED. Bhuyan et al. (2004) and Bhuyan and Bhuyan (2007) examined the low- and mid-latitude ionosphere as well as the equatorial ionization anomaly using the regularization method based on generalized singular value decomposition. They found that using this method could yield a good reconstructed image, after which they

* Corresponding author at: School of Geodesy and Geomatics, Wuhan University, Wuhan 430079, China. Tel.: +86 27 68758401.
E-mail address: ybyao@whu.edu.cn (Y. Yao).

0273-1177/$36.00 © 2013 COSPAR. Published by Elsevier Ltd. All rights reserved.
http://dx.doi.org/10.1016/j.asr.2013.09.030

further improved the method. Kunitsyn et al. (2011) and Nesterov and Kunitsyn (2011) proposed the SIRT method based on problem regularization using essentially incomplete data, and then verified the effectiveness of the method. Wen et al. (2012) proposed a regularization MART method, where the iterative algorithm was sensitive to the initial value. Garcia and Crespon (2008) and van de Kamp (2013) used a priori constraint regularization method to reconstruct IED for the ill-posed CIT. To a certain extent, these methods enhanced inversion reliability and inversion accuracy. However, these methods are less resistant to noise and tend to lose the discontinuities of IED image structures.

Considering the advantages of Total variation (TV) regularization which generally preserves discontinuities of the IED and is more resistant to noise (Vogel, 2002), it has recently been used in the CIT process. Kamalabadi and Sharif (2005) proposed an iterative algorithm for TV regularization, and demonstrated the effectiveness and reliability of this method. Lee et al. (2007, 2008) and Lee and Kamalabadi (2009) used TV regularization and Tikhonov regularization to reconstruct IED respectively, and effectively overcame the ill-posed problem at some extent. However, these methods may lead to over regularization or under regularization. Robust methods should balance these two effects. In this paper, we employ the hybrid regularization method to stabilize the solution in the presence of noise. This method is used because it generally strikes a balance between excessive and insufficient regularization, is more resistant to noise, and better preserves the discontinuities of the IED profile. Finally, a regional application of the method using simulated and real slant total electron content (STEC) data on European permanent GPS receiver networks is presented. Preliminary results, limitations, and future developments are also discussed.

2. Ionospheric tomography model

The main data source for CIT is actually coming from dual-frequency receivers of GPS. With dual-frequency GPS signals, using the carrier phase measurements at the two frequencies currently transmitted by each satellite provides a precise relative value in TEC. The code measurements are much noisier, and provide a less absolute value in TEC. After correcting for cycle slip (Blewitt, 1990) and fitting the phase measurements to the code measurement (Garcia and Crespon, 2008), the resulting error can fulfill the accuracy requirements (Lee et al., 2007). However, there are biases caused by differential delay in the receiver and satellite hardware which must be accounted for to reach this accuracy level. The STEC (Austen et al., 1988) along the ray path of the GPS signal between a satellite and a ground receiver is defined as the integrated value of the ionospheric and plasmaspheric electron density, including differential code bias (DCB), is given by

$$Y_i^j(t) = \int_{\vec{r}_i}^{\vec{r}^j} Ne(\vec{r},t)ds + B_i + B^j \quad (i = 1,\ldots,I;\ j = 1,\ldots,J) \tag{1}$$

where $Y_i^j(t)$ is the STEC; $Ne(\vec{r},t)$ is the electron density at the observation time t; I and J are the respective total number of receivers and satellites; $\vec{r}_i$ and $\vec{r}^j$ are the position of the ith ground receiver and the jth satellite; and B_i and B^j are the receiver bias and the satellite bias, respectively.

In this work, we are primarily interested in the computational domain which is divided into the ionospheric region from 100 km to 1000 km in altitude and the plasmaspheric region above 1000 km. Fig. 1 shows the schematic diagram of the computation domain of IED tomography. Note that the line integral in Eq. (1) includes the STEC contribution along the entire ray path from satellite to receiver, including the plasmasphere. Eq. (1) is separated the ionospheric and the plasmaspheric part and discretized as

$$Y_i^j(t) \approx \sum_{n=1}^{N} a_n Ne(\vec{r}_n,t) + B_i + B^j + P_i^j \tag{2}$$

where n and a denote a sampling point and the corresponding weight for the numerical integration, respectively; N is the total number of sampling points along a ray path in the ionosphere; and P_i^j is the contribution of the plasmaspheric TEC (PTEC). For our experiments, we focus on quiescent

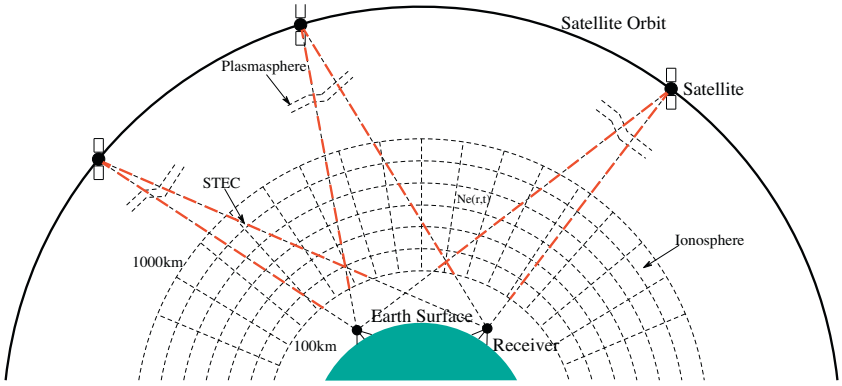

Fig. 1. Schematic diagram of the computation domain of IED tomography.

and disturbed ionospheric conditions. Eq. (2) can be written as

$$Y_i^j(t) \approx \sum_{n=1}^{N} a_n Ne(\vec{r}_n, t) + \varepsilon_i^j \tag{3}$$

where ε_i^j is the measurement and model error. We use weights a corresponding to the ray path lengths through an elliptical grid where the voxels are divided in longitude, latitude and altitude.

The set of ray path equations in (3) can be given as a discrete algebraic problem, and is expressed as follows

$$y = A \cdot x + \varepsilon \tag{4}$$

where $y \in R^{M\times 1}$ is the absolute STEC from the GPS observations values, M is the total number of STEC measurements. $A \in R^{M\times N}$ denotes the observation matrix that corresponds to the discrete grid, $x \in R^{N\times 1}$ is the IED at each voxel, and ε represents the noise.

3. Hybrid regularization method

In Eq. (4), the inverse problem is ill-posed because A is a sparse matrix. For a reliable and effective solution, Tikhonov regularization is generally used for inversion to construct the following criterion function

$$\min_x J^{\alpha}(x) = \frac{1}{2}\|Ax - y\|^2 + \frac{\alpha}{2}\Omega(x) \tag{5}$$

where α is the regularization parameter, and $\Omega(x)$ is the so-called Tikhonov stabilizer, which can change the original ill-posed problem into a well-posed problem. The stabilizer $\Omega(x)$ is chosen as $\|Lx\|^2$, where L is regularization matrix associated with a penalty operator after discretization. In this paper, L is composed of the difference matrix H along longitude and latitude, and the constraint matrix V constructed by the IRI model is in altitude. The structure of the regularization matrix encapsulates the a priori information. We want to incorporate the fact that the ionosphere is typically smoothly stratified without relying on physics-driven estimates. The choice of a discrete approximation of a derivative for the regularization matrix captures the notion of a smoothness constraint. Along the horizontal dimension, the constraint between adjacent voxels is given as $H[x_{n1}] = -x_{n1-1} + 2x_{n1} - x_{n1+1}$, where $n1$ is the voxel index. Along the vertical dimension, the constraint between adjacent voxels is given as $V[x_{n2}] = x_{n2} - \frac{x^0_{n2}}{x^0_{n2+1}} x_{n2+1}$, where $n2$ is the voxel index, and x^0_{n2} and x^0_{n2+1} are the initial value from IRI model.

This method is suitable for inversing of the continuous electron density distribution.However, one of the drawbacks of Tikhonov regularization is that suppressing the effects of high frequency noise, and also reduces the high-frequency energy in the IED profile,thereby blurring edges or the steep gradients, which results in high-gradient areas where the gradient of the reference profile does not match that of the true IED profile. However, TV regularization is a nonlinear technique that effectivelyattempts to be more resistant to noise and preservesthe discontinuities of the IED (Rudin et al., 1992; Vogel, 2002). In view of the respective advantages of the two different stabilizers, we integrate Tikhonov regularization with total variation regularization in the experimental study. A new criterion function is constructed as follows

$$\min_x J^{\alpha,\beta}(x) = \frac{1}{2}\|Ax - y\|^2 + \frac{\alpha}{2}\|Lx\|^2 + \beta \mathrm{TV}(x) \tag{6}$$

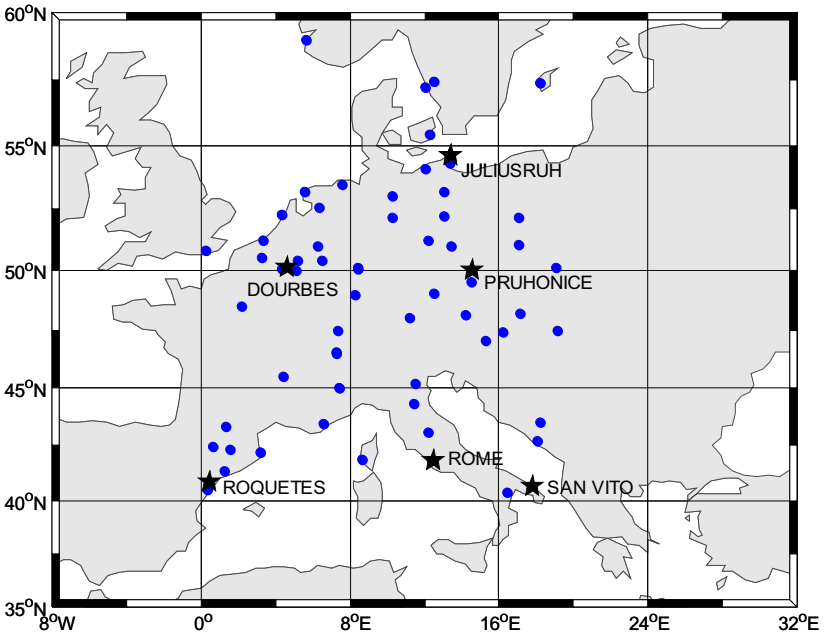

Fig. 2. Map of IGS European observation stations and ionosondes.

where α and β are the regularization parameters. To overcome the non-differentiability of the stabilizer $\mathrm{TV}(x)$ at the origin, we take an approximation to the stabilizer. This process yields the approximation $\mathrm{TV}(x)$, which is valid for a smooth function x defined on the unit interval in three dimensions

$$\mathrm{TV}(x) = \frac{1}{2}\sum_{s=1}^{N_s-1}\sum_{t=1}^{N_t-1}\sum_{z=1}^{N_z-1}\left((D_s x)^2 + (D_t x)^2 + (D_z x)^2 + \tau\right)^{1/2} \tag{7}$$

where N_s, N_t and N_z are the number of grids along longitude, latitude and altitude respectively and $N = N_s N_t N_z$; τ is a small constant which is an artificial parameter added to ensure differentiability at points; D_s, D_t and D_z are the grid operators. Along the horizontal direction, $D_s x = x_{s+1,t,z} - x_{s,t,z}$ and $D_t x = x_{s,t+1,z} - x_{s,t,z}$. Along the vertical direction, $D_z x = x_{s,t,z+1} - x_{s,t,z}$. From Eq. (7), we obtain the gradient

$$\nabla \mathrm{TV}(x) = \begin{bmatrix} D_1^T & D_2^T & D_3^T \end{bmatrix} \begin{bmatrix} W(x) & 0 & 0 \\ 0 & W(x) & 0 \\ 0 & 0 & W(x) \end{bmatrix} \begin{bmatrix} D_1 \\ D_2 \\ D_3 \end{bmatrix}$$
$$x = D^T W(x) D x \tag{8}$$

where $W(x)$ is a $(N_s-1)(N_t-1)(N_z-1) \times (N_s-1)(N_t-1)(N_z-1)$ diagonal matrix with elements $\left((D_s x)^2 + (D_t x)^2 + (D_z x)^2 + \tau\right)^{-1/2}$; D_1, D_2 and D_3 denote the resulting $(N_s-1)(N_t-1)(N_z-1) \times N_s N_t N_z$ matrices corresponding to the grid operators D_s, D_t and D_z. From Eq. (6), we obtain the gradient

$$\nabla J^{\alpha,\beta}(x) = A^T p(Ax - y) + \alpha L^T L x + \beta D^T W(x) D x \tag{9}$$

where p is the weight matrix of the STEC measurements, which is determined by the satellite's elevation angle and this method is introduced in detail by Gao et al. (2005). To obtain the Hessian of $J^{\alpha,\beta}(x)$, we use Eq. (6).

$$H_{J,x} = A^T pA + \alpha L^T L + \beta D^T W(x) D \tag{10}$$

We use the Gauss–Newton method to solve the minimization problem of hybrid regularization.

$$x^{k+1} = x^k - \lambda H_{J,x^k}^{-1} \nabla J(x^k) \tag{11}$$

where k is the iteration step number, and λ is the attenuation factor. In this paper, we use the attenuation factor, which is set to 0.2 that is an empirical value. Selecting the optimal value of the regularization parameter, particularly in operational use, is important when using our inversion model. In this paper, we use the regularization parameters in Eq. (10), which are expressed as follows (Zibetti et al., 2008)

$$\alpha = \sqrt{\mathrm{tr}(A^T pA)} \Big/ \sqrt{2\mathrm{tr}(L^T L)} \tag{12}$$

$$\beta = \sqrt{\mathrm{tr}(A^T pA)} \Big/ \sqrt{2\mathrm{tr}(D^T W(x) D)} \tag{13}$$

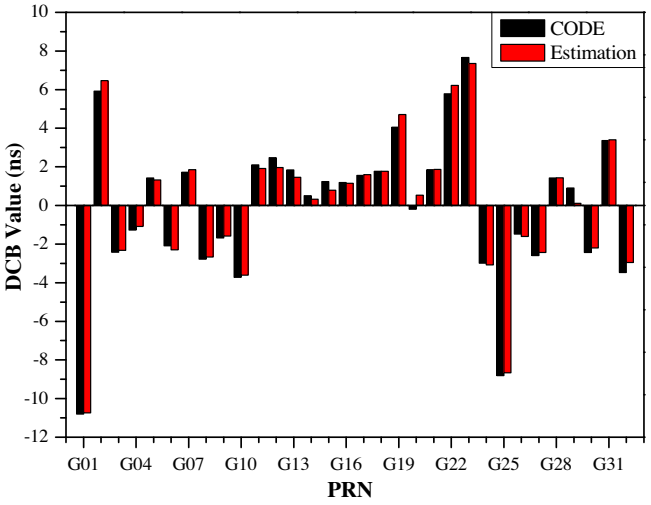

Fig. 3. Comparison of the estimated and the CODE differential code bias in satellites.

According to the inversion theory, the choice of these two parameters should be related to noise level, which is significant in finding a trade-off to balance the data fitting and penalty item.

4. Experimental examples

To test the validity and reliability of the hybrid regularization method used to reconstruct the IED, we select data ranging in longitude (0°E to 20°E), latitude (40°N to 60°N) and altitude (100 km to 1000 km) for inversion. The spatial resolution along the longitude, latitude and altitude is $2° \times 2° \times 50$ km. Thus, the total number of grids is 2299. A small angular velocity of high orbital satellites significantly deteriorates the experiment geometry and possibilities of the tomography (Kunitsyn et al., 1997). During the course of the CIT experiment, we have taken one hour

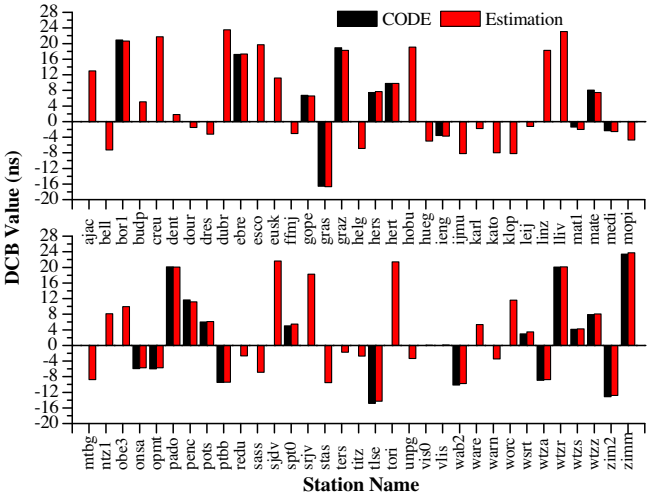

Fig. 4. Comparison between the estimated and the CODE differential code bias in receivers.

Table 1
Error analysis of IED reconstruction using the two methods at various longitudes (unit: 10^{10} el/m^3).

Error	Hybrid regularization			Tikhonov regularization		
	4°E	10°E	16°E	4°E	10°E	16°E
Maximum absolute error	2.76	3.84	1.49	5.58	7.23	6.16
Average absolute error	0.04	0.04	0.04	0.08	0.06	0.11
RMSE	0.21	0.29	0.19	0.49	0.62	0.62

for the observation time interval and used one hour GPS observation data to do our experiments. We select the reference stations from the area of the European IGS global permanent network and use the data of the ionosonde station Pruhonice (14.60°E, 50.00°N) to test and verify independently. The GPS station distribution of the setting region is shown in Fig. 2 ("•" for IGS reference stations, "★" for ionosonde stations).

As the main error source when obtaining STEC by using GPS dual frequency observations, the differential code bias (DCB) is the basis for ensuring reliable computerized ionospheric tomography results and must therefore be considered when calculating the STEC. In this paper, we use a high-precision, single-layer ionospheric model commonly used internationally to estimate the system DCB (Arikan et al., 2008; Jin et al., 2008). To get more precise DCB estimates, the differential pseudorange observations need to be smoothed. After smoothing, differential pseudorange observations can be used to extract reliable estimates using the least squares method (Jin et al., 2008).

Fig. 3 and 4 show the satellite and receiver DCB estimation values compared with the DCB values provided by the CODE center on 8 April 2012, respectively. These two Figures show that the DCB estimation values are very close to the DCB provided by the CODE center. The standard deviation between the 32 satellites DCB estimation values and the CODE center data is 0.32 ns, and the maximum difference is 0.79 ns. At the same time, we compute the DCB values of 66 receivers, of which the CODE center only provides data 27 stations. The standard deviation between these two sets of data is 0.34 ns, and the maximum difference is 0.67 ns. Therefore, this result demonstrates that the satellite and receiver DCB values we calculated are highly precise, thereby guaranteeing the reliability of the CIT.

4.1. Experiment using simulated data

In this section, a set of IED distributions at 14:00 UT, 8 April 2012 is provided by the IRI2007 model, and precise known positions of GPS satellites and ground receivers selected from the European IGS global permanent network are used to establish the matrix A of Eq. (4). The electron densities x_{IRI}, which are as the prior values, are generated from the IRI2007 model. Meanwhile, a small amount of random noise ε, which should follow Gaussian distribution $\varepsilon \sim N(0, 0.01)$, is added to the simulated STEC values Ax_{IRI} in order to obtain more realistic values y_{simu}

$$y_{simu} = Ax_{IRI} + \varepsilon \tag{14}$$

To examine the inversion results of our reconstruction method, we design a contrast experiment by using the hybrid regularization and Tikhonov regularization methods. First, we do not exert any constraints on the observation equation to enable an analysis of how the constraint matrix affects the inversion results, and the condition number of the regularization matrix A^TpA in Eq. (9) is 4.2606×10^8. However, the number of regularization matrix $A^TpA + \alpha L^TL$ in Eq. (9) is 1.1538×10^3 when applying Tikhonov regularization, where as the number of regularization matrix $A^TpA + \alpha L^TL + \beta D^TW(x)D$ in Eq. (9) is 2.2872×10^2 when further conducting hybrid regularization. These values are significantly reduced. Therefore, the normal matrix is significantly improved after regularization.

Tables 1 and 2 provide the inversion results of the error statistics of the two methods at various longitudes and heights, respectively. The hybrid regularization errors are all smaller than those of single Tikhonov regularization at 4°E, 10°E and 6°E in longitude and at different heights, indicating that hybrid regularization is an effective method of reconstructing IED. From the two tables, it can be seen that the reconstruction errors of hybrid regularization method area bout twice less than those of single Tikhonov regularization method as a whole. Thus, we confirm the validity of hybrid regularization method. Meanwhile, the statistical results show that during hybrid regularization, the average absolute error of IED in all pixels is about 2.0×10^9 el/m^3, the maximum absolute value of IED is about 6.7×10^{10} el/m^3, and the peak electron density of

Table 2
Error analysis of IED reconstruction using the two methods at various heights (unit: 10^{10} el/m^3).

Altitude (km)	Hybrid regularization			Tikhonov regularization		
	Maximum absolute error	Average absolute error	RMSE	Maximum absolute error	Average absolute error	RMSE
200	3.34	0.10	0.50	8.14	0.18	1.11
300	3.58	0.08	0.46	9.23	0.18	0.87
400	1.88	0.06	0.26	8.57	0.10	0.99
500	1.50	0.03	0.21	7.58	0.10	0.76
600	1.01	0.03	0.15	6.00	0.09	0.60

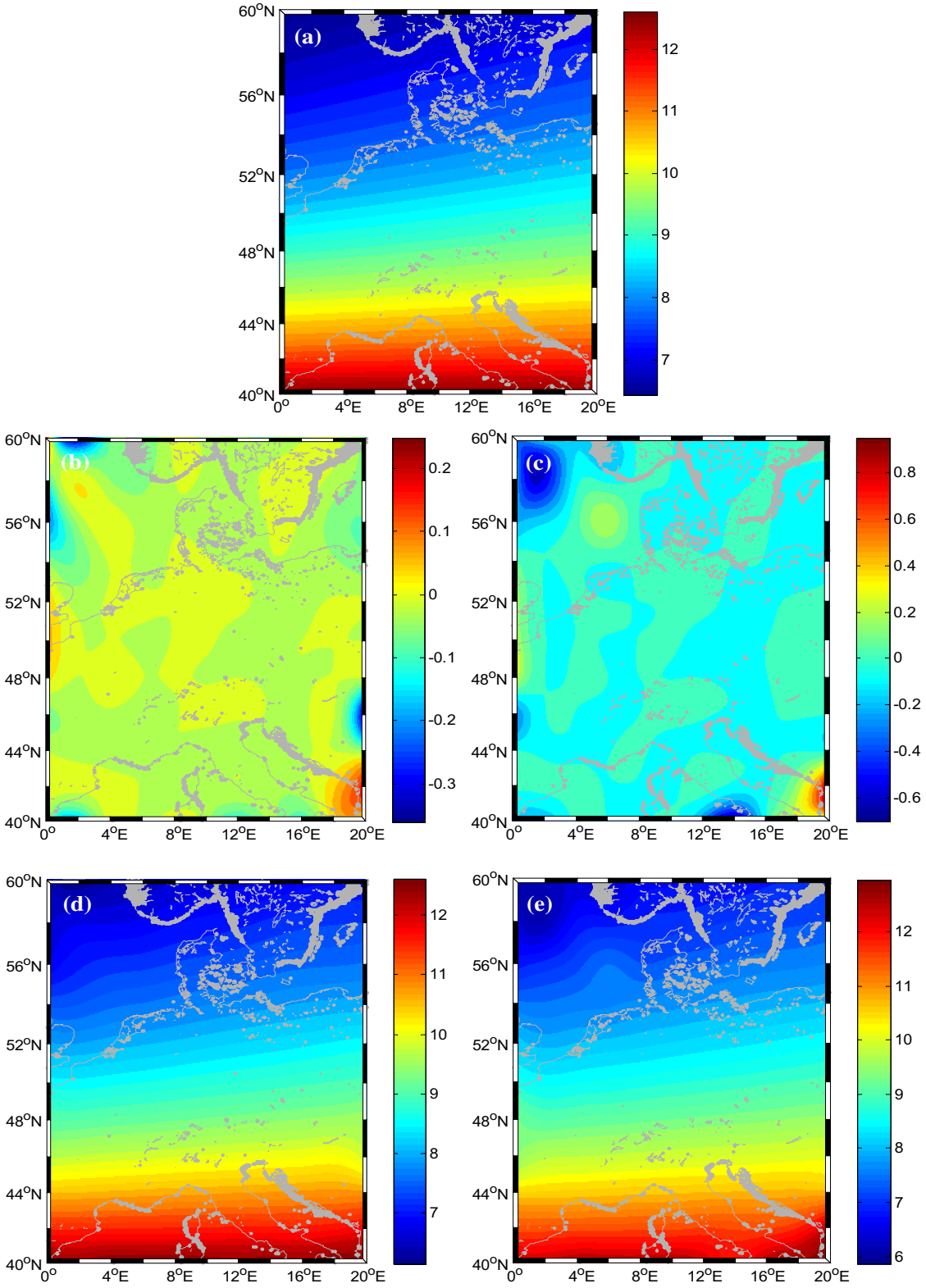

Fig. 5. Estimated IED for hybrid regularization (left panel) and Tikhonov regularization (right panel) at 300 km on 8 April 2012 at 14:00 UT (unit: 10^{11} el/m^3). (a) is IRI. (b) and (c) are error term. (d) and (e) are estimated electron density.

the ionosphere is 1.3×10^{12} el/m^3. However, the above two error terms are smaller than the peak electron density of the ionosphere, which confirms the reliability of the inversion results when using hybrid regularization.

The estimation values of the electron density for the two methods at a height of 300 km on 8 April 2012 at 14:00 UT are shown in Fig. 5. The IED and its error distribution, as reconstructed by hybrid regularization, are shown in

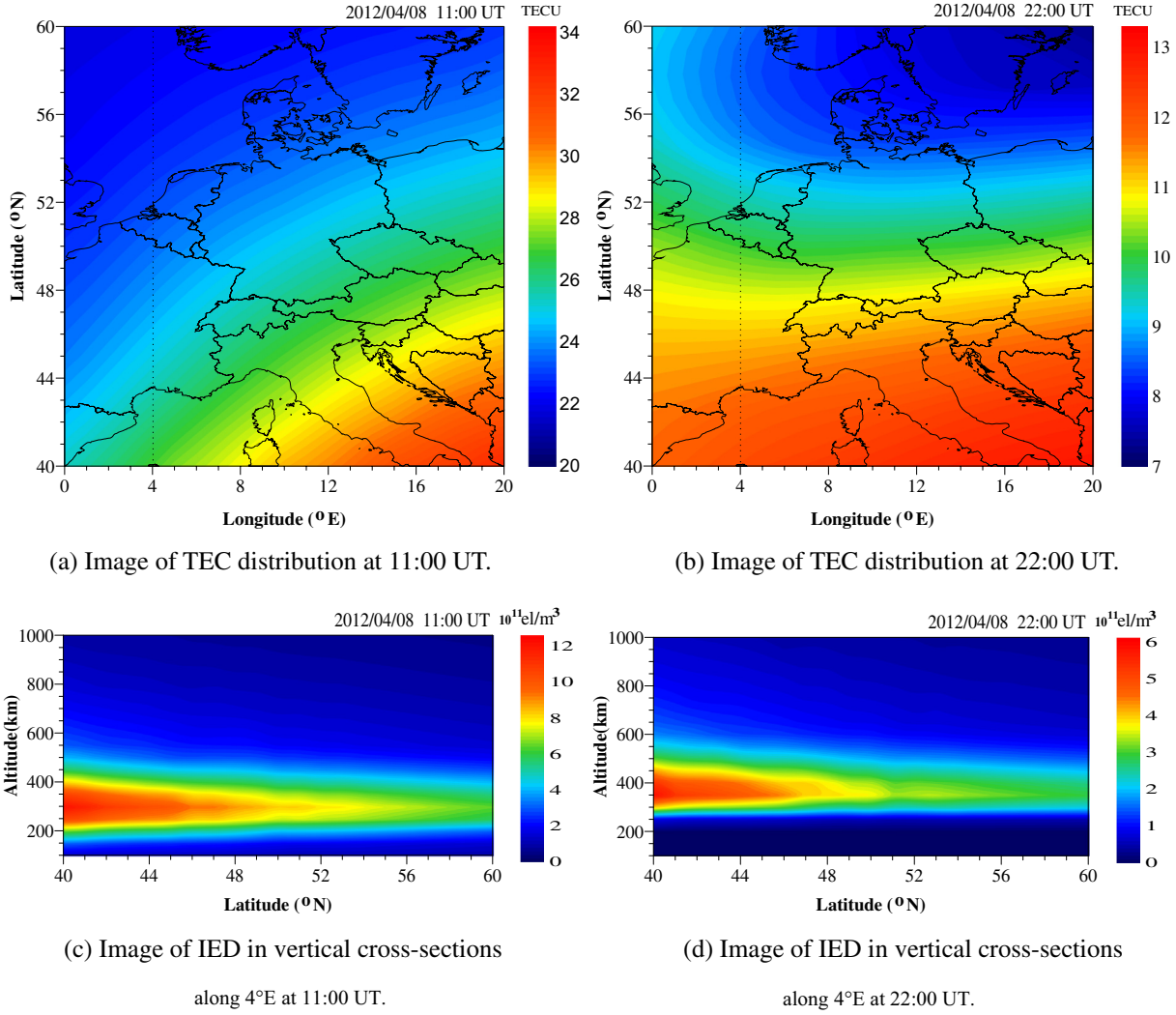

(a) Image of TEC distribution at 11:00 UT.

(b) Image of TEC distribution at 22:00 UT.

(c) Image of IED in vertical cross-sections along 4°E at 11:00 UT.

(d) Image of IED in vertical cross-sections along 4°E at 22:00 UT.

Fig. 6. TEC distribution and reconstruction of IED on 8 April 2012.

Fig. 5(d) and (b), respectively. The IED and its error distribution, as reconstructed by using Tikhonov regularization, are shown in Fig. 5(e) and 5(c), respectively. We can conclude from these figures that compared with Tikhonov regularization method, the hybrid regularization method can derive more reliable values and obtain results closer to the true values.

4.2. Reconstruction of the IED from real observation data

The above conclusions are based on simulated data. We should use the real data to further test the validity and reliability of the hybrid regularization method. In the section, we apply it to a model problem, in which the electron density distribution is generated by using the IRI extended to Plasmasphere (IRI-Plas) from IZMIRAN (Gulyaeva and Bilitza, 2012).We use the IZMIRAN model to obtain the background electron density distribution of the plasmasphere $Ne(\vec{r}_{n_p}, t)$ as true values. The plasmaspheric contribution for each ray is calculated as $P_i^j = \sum_{n_p=1}^{N_p} \gamma_{n_p} Ne(\vec{r}_{n_p}, t)$, where n_p and γ denote a sampling point and the corresponding weight for the numerical integration, respectively; N_p is the total number of sampling points along a ray path in the plasmasphere. This value is then

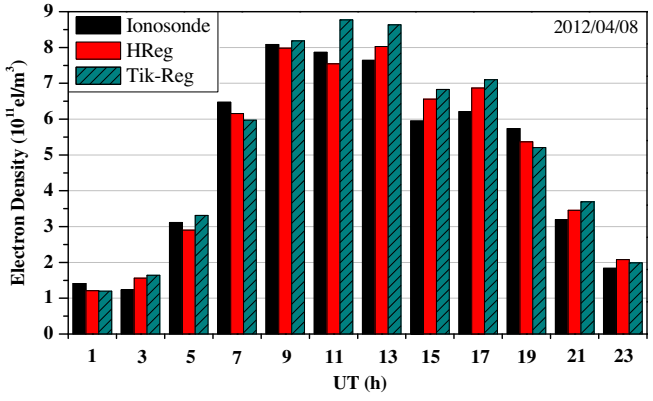

Fig. 7. Comparison of NmF2 values obtained from CIT and ionosonde data from Pruhonice ionosonde.

Table 3
Relative error analysis of NmF2 reconstruction using the two methods and from IRI-Plas.

UT	1	3	5	7	9	11	13	15	17	19	21	23
Altitude (km)	311	313	226	256	260	287	266	254	282	295	278	331
IRI-Plas_RE (%)	89.94	69.51	0.78	11.11	2.04	18.89	19.81	47.92	31.80	5.42	25.33	75.57
HReg_RE (%)	14.20	26.94	6.87	4.95	1.29	4.07	5.05	10.32	10.64	6.37	8.26	13.03
Tik-Reg_RE (%)	15.19	33.44	6.21	7.79	1.22	11.53	12.98	14.85	14.37	9.22	15.65	7.99

subtracted from the total STEC to obtain the STEC in the ionosphere. And the proposed method is applied to the analysis of real observation data under quiescent and disturbed ionospheric conditions.

4.2.1. Quiescent ionospheric conditions

On 8 April 2012, ionosphere is under quiescent conditions. Fig. 6 shows the inversion results with the spatial distribution of the actual TEC. The left two figures give the distribution at 11:00 UT, and the right two figures give the distribution at 22:00 UT, which represent the results when electron density is comparatively large at day and when electron density is comparatively small at night, respectively. (a) and (b) are the actual TEC distributions in space, and (c) and (d) are the vertical profiles at 4°E longitude. These figures indicate that the electron density reconstructed using hybrid regularization gradually decreases as latitude increases, which agrees with the actual space TEC distributions and trends, thereby illustrating the validity of the method.

To gain a thorough understanding of the reliability of the inversion results, we compared the results with ionosonde data. Fig. 7 shows that the different NmF2 values derived from inversion using hybrid and Tikhonov regularization as well as ionosonde data during all 12 time intervals in a day. Compared with Tikhonov regularization results, the results obtained using hybrid regularization are closer to the ionosonde data as a whole. The relative errors indicate the percentage of error in the IRI-Plas prediction and reconstructed NmF2values with respect to the ionosonde results in Table 3, calculated as $\frac{|\mathrm{NmF2}_{recon}-\mathrm{NmF2}_{iono}|}{\mathrm{NmF2}_{iono}}\cdot 100$. It is seen that the relative error of IRI-Plas prediction is high, the relative error of estimated NmF2 reduces significantly by the two methods and that of the proposed method reduces even more as a whole. This confirms the accurate estimation of CIT using the proposed method.

This paper uses the observation data of the ionosonde to check the computerized ionospheric tomography results of the method. Fig. 8 compares the profiles derived from the Pruhonice ionosonde at the different time with the reconstruction results derived from the two methods and the results of the IRI-Plas model. Fig. 8(a) is the comparison of the reconstructed electronic density profile at 11:00 UT, and Fig. 8(b) is the comparison of the reconstructed electronic density profile at 21:00 UT. The figure shows that the peak electron density of the F2 layer is consistent with the ionosonde observation results as a whole. The peak height is the same as that of ionosonde in Fig. 8(a). However, some differences remain between the peak height of the F2 layer and ionosonde in Fig. 8(b). Owing to GPS observation noise, ionospheric space discretization error, station geometry restrictions, and so on, the vertical resolution of the inversion results still need to be improved. This result shows that CIT processes with additional horizontal and vertical constraints to improve spatial structure of electron density are insufficient, such that other methods are required to increase the amount of observation information.

4.2.2. Disturbed ionospheric conditions

Now we present several examples of CIT imaging of regional distributions of IED during the geomagnetic storm on 24 August 2005. Fig. 9 shows two examples of

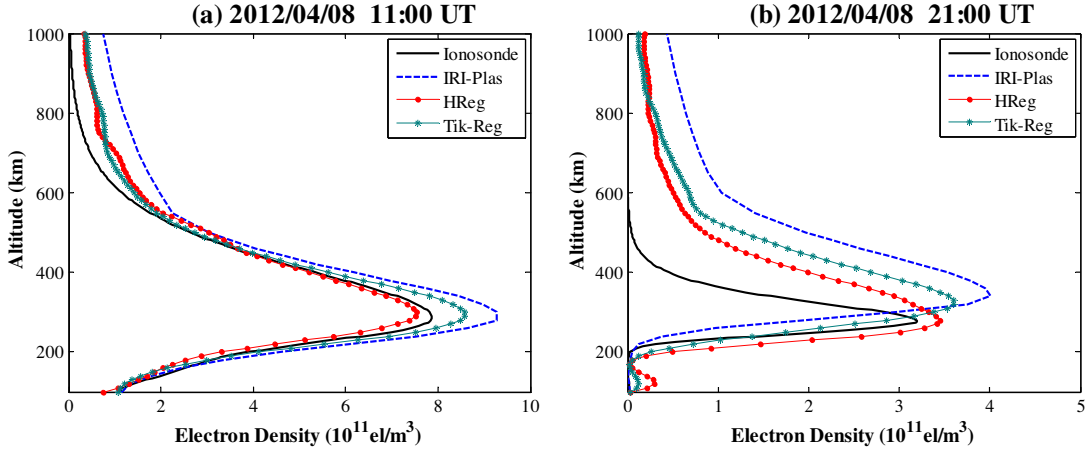

Fig. 8. Comparison of estimated IED profiles by two methods with IED profiles from Pruhonice ionosonde on 8 April 2012.

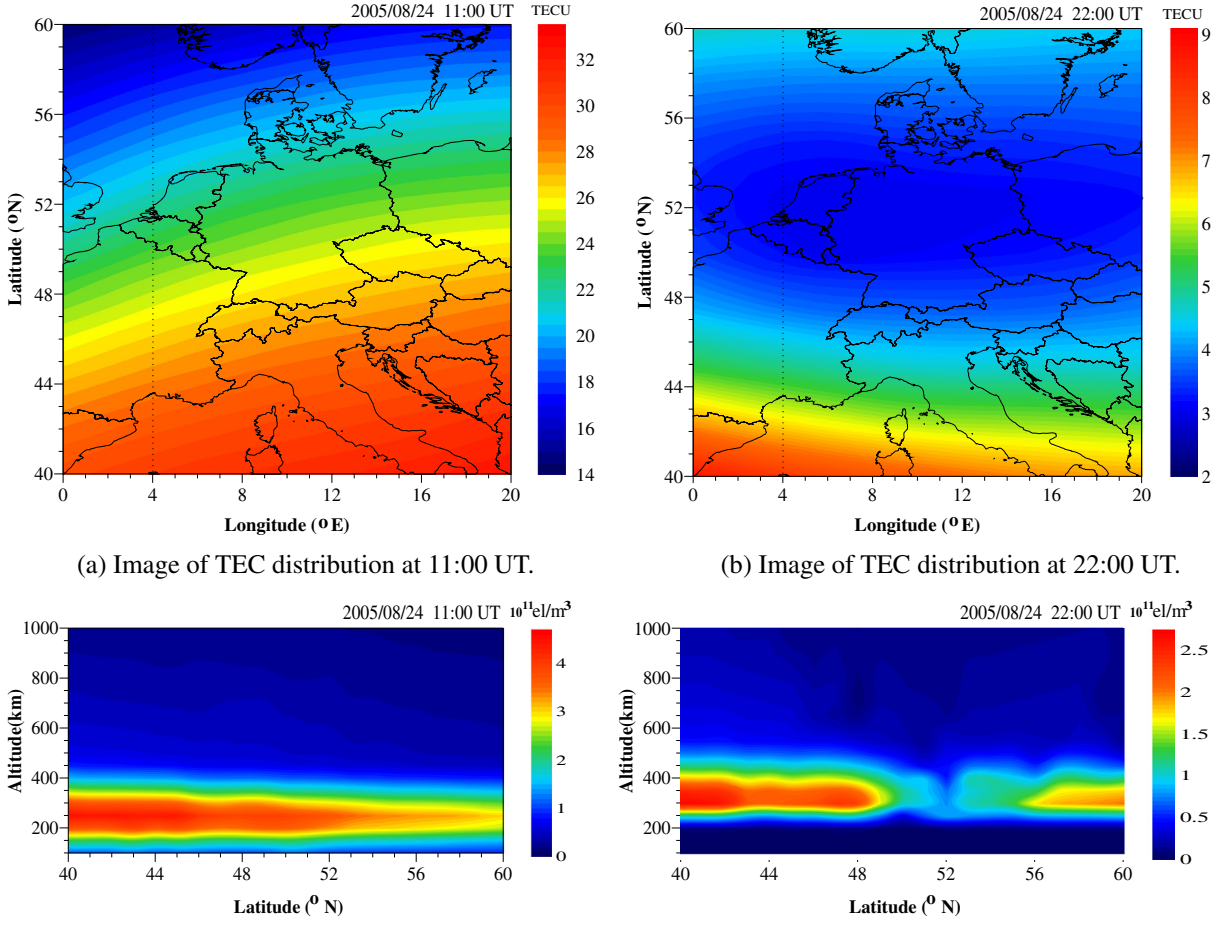

(a) Image of TEC distribution at 11:00 UT.

(b) Image of TEC distribution at 22:00 UT.

(c) Image of IED in vertical cross-sections along 4°E at 11:00 UT.

(d) Image of IED in vertical cross-sections along 4°E at 22:00 UT.

Fig. 9. TEC distribution and reconstruction of IED on 24 August 2005.

tomographic images over the part of Europe. These examples have been chosen and are for 11:00 UT and 22:00 UT. The three-dimensional images have been integrated through and contoured to show the spatial distribution of vertical TEC on Fig. 9(a) and (b). Fig. 9(a) shows a gradient to the southeast reaching TEC values of about 33 TECU. Fig. 9(b) shows the TEC values significantly decrease and appear ionospheric trough at around latitude 52°. For both TEC images, a cross section of the IED at grid longitude 4° is shown on Fig. 9(c) and (d). Both cross sections show that the IED reaches a maximum at around 250 km and 350 km at daytime and nighttime, respectively. Fig. 9(d) shows the strong change is at around grid latitude 52°.

Fig. 10 and Table 4 compare the Ionosonde, IRI-Plas and NmF2 estimated by two method as well as their relative errors. The relative errors demonstrate the percentage of error in the IRI-Plas prediction and estimated NmF2 with respect to the results of Pruhonice ionosonde. From the figure, the NmF2 estimated by hybrid regularization method closely approximates the ionosonde measurements as a whole. From the table, it can be seen that the relative error of IRI-Plas prediction is high, the relative error of estimated NmF2 reduces significantly by the two methods and that of the proposed method reduces even more as a whole. This confirms the accurate estimation using the proposed method under disturbed ionospheric conditions.

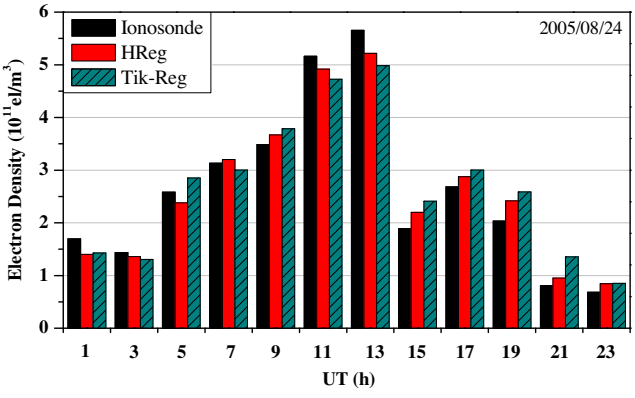

Fig. 10. Comparison of NmF2 values obtained from CIT and ionosonde data from Pruhonice ionosonde.

Table 4
Relative error analysis of NmF2 reconstruction using the two methods and from IRI-Plas.

UT	1	3	5	7	9	11	13	15	17	19	21	23
Altitude (km)	330	236	280	241	285	348	338	199	241	353	397	371
IRI-Plas_RE (%)	26.59	23.69	25.44	4.22	11.60	23.27	36.94	77.09	40.41	106.50	241.15	134.66
HReg_RE (%)	17.41	5.38	7.84	2.20	5.30	4.74	7.68	16.66	7.24	18.79	17.76	23.06
Tik-Reg_RE (%)	15.85	8.95	10.41	4.13	8.54	8.47	11.83	22.83	11.93	27.09	67.97	24.42

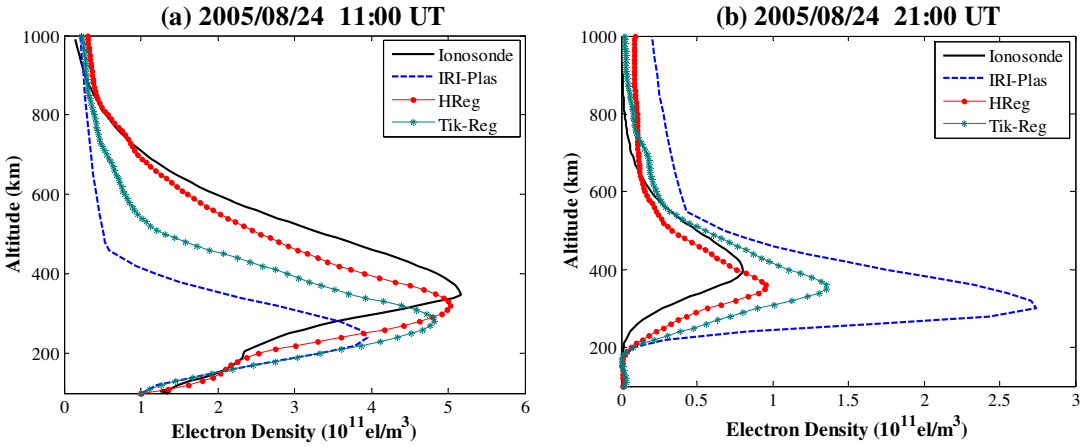

Fig. 11. Comparison of estimated IED profiles by two methods with IED profiles from Pruhonice ionosonde on 24 August 2005.

Fig. 11 shows the compared results. From the figure, it can be seen that the IED profile obtained from the hybrid regularization method matches the ionosonde profile better than those obtained from the Tikhonov regularization method as a whole. This further validates that the proposed method is superior to the Tikhonov regularization method for the tomographic reconstruction of IED based on actual GPS observations under disturbed ionospheric conditions. In Fig. 11(a), the peak height of the proposed method is lower than that of the ionosonde. In Fig. 11(b), the peak height of the proposed method is slightly lower than that of the ionosonde. However, at the top of the ionosphere, the electron densities of the Tikhonov regularization method are closer to the ionosonde.

5. Conclusion

Regularization is an efficient means of solving ill-posed inversion problems. A priori information, which included the regularization items, can improve the ill-posedness of the inversion problem, thereby obtaining highly-accurate CIT reconstruction results. In this paper, we propose a hybrid regularization method for studying the ill-posed CIT problems. Validated by experiments, this method can improve the performance of Tikhonov regularization. In the future, an efficient numerical calculation technique will be needed means to ameliorate hybrid regularization and reducing the burden of calculation. In addition, ill-posed problems cannot be completely solved without obtaining adequate observation information.

Acknowledgements

The authors would like to thank the IGS for providing the GPS data and the GIRO for providing the ionosonde data, and Tamara Gulyaeva and Dieter Bilitza for providing free use of the IZMIRAN plasmasphere model. The authors also thank reviewers for their assistance in evaluating this paper. This research was supported by the National Natural Science Foundation of China (41174012 and 41274022) and The National High Technology Research and Development Program of China (2013AA122502).

References

Arikan, O., Arikan, F., Erol, C.B., 2007. Computerized ionospheric tomography with the IRI model. Adv. Space Res. 39, 859–866.

Arikan, F., Nayir, H., Sezen, U., Arikan, O., 2008. Estimation of single station interfrequency receiver bias using GPS-TEC. Radio Sci. 43, RS4004. http://dx.doi.org/10.1029/2007RS003785.

Austen, J.R., Franke, S.J., Liu, C.H., Yeh, K.C., 1986. Application of computerized tomography techniques to ionospheric research. In: Tauriainen, A. (Ed.), Radio Beacon Contributions to the Study of Ionization and Dynamics of the Ionosphere and to Corrections to Geodesy and Technical Workshop. Oulu, Finland, Part 1, pp. 25–35.

Austen, J.R., Franke, S.J., Liu, C.H., 1988. Ionospheric imaging using computerized tomography. Radio Sci. 23, 299–307.

Bhuyan, K., Singh, S.B., Bhuyan, P.K., 2004. Application of generalized singular value decomposition to ionospheric tomography. Ann. Geophys. 22, 3437–3444.

Bhuyan, K., Bhuyan, P.K., 2007. International reference ionosphere as a potential regularization profile for computerized ionospheric tomography. Adv. Space Res. 39, 851–858.

Blewitt, G., 1990. An automatic editing algorithm for GPS data. Geophys. Res. Lett. 17, 199–202.

Gao, C., Zhao, Y., Wan, D., 2005. The weight determination of the double difference observation in GPS carrier phase positioning. Sci. Surv. Mapp. 30, 28–32 (in Chinese).

Garcia, R., Crespon, F., 2008. Radio tomography of the ionosphere: analysis of an underdetermined, ill-posed inverse problem, and regional application. Radio Sci. 43, RS2014. http://dx.doi.org/10.1029/2007RS003714.

Gulyaeva, T.L., Bilitza, D., 2012. Towards ISO standard earth ionosphere and plasmasphere model. In: New Developments in the Standard Model, NOVA, Hauppauge, New York, pp. 1–39.

Hirooka, S., Hattori, K., Takeda, T., 2011. Numerical validations of neural-network-based ionospheric tomography for disturbed ionospheric conditions and sparse data. Radio Sci. 46, RS0F05. http://dx.doi.org/10.1029/2011RS004760.

Hobiger, T., Kondo, T., Koyama, Y., 2008. Constrained simultaneous algebraic reconstruction technique (C-SART) – a new and simple algorithm applied to ionospheric tomography. Earth Planets Space 60, 727–735.

Jin, S., Luo, O.F., Park, P., 2008. GPS observations of the ionospheric F2-layer behavior during the 20th November 2003 geomagnetic storm over South Korea. J. Geod. 82, 883–892. http://dx.doi.org/10.1007/s00190-008-0127-x.

Kamalabadi, F., Sharif, B., 2005. Robust regularized tomographic imaging with convex projections. In: Proc. IEEE International Conference on Image Processing (ICIP'05), Genova, Italy, vol. 2, pp. 205–208.

Kunitsyn, V.E., Andreeva, E.S., Razinkov, O.G., 1997. Possibilities of the near-space environment radio tomography. Radio Sci. 32, 1953–1963.

Kunitsyn, V.E., Nesterov, I.A., Padokhin, A.M., Tumanova, Y.S., 2011. Ionospheric radio tomography based on the GPS/GLONASS navigation systems. J. Commun. Technol. Electron. 56, 1269–1281.

Lee, J.K., Kamalabadi, F., Makela, J.J., 2007. Localized three-dimensional ionospheric tomography with GPS ground receiver measurements. Radio Sci. 42, RS4018. http://dx.doi.org/10.1029/2006RS003543.

Lee, J.K., Kamalabadi, F., Makela, J.J., 2008. Three-dimensional tomography of ionospheric variability using a dense GPS receiver array. Radio Sci. 43, RS3001. http://dx.doi.org/10.1029/2007RS003716.

Lee, J.K., Kamalabadi, F., 2009. GPS-based radio tomography with edge-preserving regularization. IEEE Trans. Geosci. Remote Sens. 47, 312–324.

Ma, X.F., Maruyama, T., 2005. Three-dimensional ionospheric tomography using observation data of GPS ground receivers and ionosonde by neural network. J. Geophys. Res. 110, A05308. http://dx.doi.org/10.1029/2004JA010797.

Mitchell, C.N., Spencer, P.S.J., 2003. A three-dimensional time-dependent algorithm for ionospheric imaging using GPS. Ann. Geophys. 46, 687–696.

Nesterov, I.A., Kunitsyn, V.E., 2011. GNSS radio tomography of the ionosphere: the problem with essentially incomplete data. Adv. Space Res. 47, 1789–1803.

Nygren, T., 1997. Stochastic inversion in ionospheric radiotomography. Radio Sci. 32, 2359–2372.

Pryse, S.E., Kersley, L., Mitchell, C.N., Spencer, P.S.J., Williams, M.J., 1998. A comparison of reconstruction techniques used in ionospheric tomography. Radio Sci. 33, 1767–1779.

Raymund, T.D., Austen, J.R., Franke, S.J., Liu, C.H., Klobuchar, J.A., Stalker, J., 1990. Application of computerized tomography to the investigation of ionospheric structures. Radio Sci. 25, 771–789.

Rudin, L.I., Osher, S., Fatemi, E., 1992. Nonlinear total variation based noise removal algorithms. Physica D 60, 259–268.

van de Kamp, M.M.J.L., 2013. Medium-scale 4-D ionospheric tomography using a dense GPS network. Ann. Geophys. 31, 75–89.

Vogel, C.R., 2002. Computational Methods for Inverse Problems. SIAM, Philadephia, PA.

Wen, D.B., Yuan, Y.B., Ou, J., Huo, X., Zhang, K., 2007. Three-dimensional ionospheric tomography by an improved algebraic reconstruction technique. GPS Solut. 11, 251–258.

Wen, D.B., Yuan, Y.B., Ou, J., Zhang, K., Liu, K., 2008. A hybrid reconstruction algorithm for 3-D ionospheric tomography. IEEE Trans. Geosci. Remote Sens. 46, 1733–1739.

Wen, D.B., Wang, Y., Norman, R., 2012. A new two-step algorithm for ionospheric tomography solution. GPS Solut. 16, 89–94.

Zibetti, M., Bazan, F., Mayer, J., 2008. Determining the regularization parameters for super-resolution problems. Signal Process. 88, 2890–2901.